Heliyon 9 (2023) e21309

Contents lists available at ScienceDirect

Heliyon

journal homepage: www.cell.com/heliyon

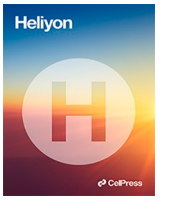

Protective effect and mechanism of procyanidin B2 against hypoxic injury of cardiomyocytes

Zhimin Xue [a], Danyu Wu [a], Jiefang Zhang [a], Yiwen Pan [a], Rongsheng Kan [a], Jing Gao [a], Binquan Zhou [a,*]

[a] *Department of Cardiology, Sir Run Run Shaw Hospital, Zhejiang University School of Medicine, Hangzhou, China*

ARTICLE INFO

Keywords:
Coronary heart disease
Procyanidin B2
Cardiomyocyte hypoxia
Oxidative stress
Apoptosis

ABSTRACT

Background: Cardiomyocyte ischemia and hypoxia are important causes of oxidative stress damage and cardiomyocyte apoptosis in coronary heart disease (CHD). Epidemiological investigation has shown that eating more plant-based foods, such as vegetables and fruits, may significantly decrease the risk of CHD. As natural antioxidants, botanicals have fewer toxic side effects than chemical drugs and have great potential for development. Procyanidin B2 (PB2) is composed of flavan-3-ol and epicatechin and has been reported to have antioxidant and anti-inflammatory effects. However, whether PB2 exerts protective effects on hypoxic cardiomyocytes has remained unclear. This study aimed to explore the protective effect of PB2 against cardiomyocyte hypoxia and to provide new treatment strategies and ideas for myocardial ischemia and hypoxia in CHD. *Methods and results:* A hypoxic cardiomyocyte model was constructed, and a CCK-8 assay proved that PB2 had a protective effect on cardiomyocytes in a hypoxic environment. DCFH fluorescence staining, DHE staining, and BODIPY lipid oxidation assessment revealed that PB2 reduced the oxidative stress levels of cardiomyocytes under hypoxic conditions. TUNEL staining, Annexin V/PI fluorescence flow cytometry, and Western blot analysis of the expression of the apoptosis marker protein cleaved caspase-3 confirmed that PB2 reduced cardiomyocyte apoptosis under hypoxic conditions. JC-1 staining indicated that PB2 reduced the mitochondrial membrane potential of cardiomyocytes under hypoxia. In addition, transcriptomic analysis proved that the expression of 158 genes in cardiomyocytes was significantly changed after PB2 was added during hypoxia, of which 53 genes were upregulated and 105 genes were downregulated. GO enrichment analysis demonstrated that the activity of cytokines, extracellular matrix proteins and other molecules was changed significantly in the biological process category. KEGG enrichment analysis showed that the IL-17 signaling pathway and JAK-STAT signaling pathway underwent significant changes. We also performed metabolomic analysis and found that the levels of 51 metabolites were significantly changed after the addition of PB2 to cardiomyocytes during hypoxia. Among them, 39 metabolites exhibited increased levels, while 12 metabolites exhibited decreased levels. KEGG enrichment analysis showed that cysteine and methionine metabolism, arginine and proline metabolism and other metabolic pathways underwent remarkable changes. *Conclusion:* This study proves that PB2 can reduce the oxidative stress and apoptosis of cardiomyocytes during hypoxia to play a protective role. Transcriptomic and metabolomic analyses preliminarily revealed signaling pathways and metabolic pathways that are related to its

* Corresponding author.Department of Cardiology, Sir Run Run Shaw Hospital, Zhejiang University School of Medicine, 3 East Qingchun Road, Hangzhou 310016, Zhejiang Province, China.
E-mail address: zhoubinquan@zju.edu.cn (B. Zhou).

https://doi.org/10.1016/j.heliyon.2023.e21309
Received 18 July 2023; Received in revised form 18 October 2023; Accepted 19 October 2023
Available online 20 October 2023

protective mechanism. These findings lay a foundation for further research on the role of PB2 in the treatment of CHD and provide new ideas and new perspectives for research on PB2 in the treatment of other diseases.

1. Introduction

Coronary heart disease (CHD) is closely related to myocardial ischemia and hypoxia caused by coronary artery lumen stenosis or occlusion and has become the most dangerous cardiovascular diseases causing death and disability in China today. Myocardial ischemia occurs when the blood flow required for myocardial metabolism exceeds the supply of coronary arteries. Significant increases in apoptosis are observed during myocardial ischemia [1]. Although there are many treatment methods for CHD, such as percutaneous coronary intervention (PCI) and antiplatelet drug, β-blocker and angiotensin-converting enzyme inhibitor (ACEI) treatment, these methods have their own limitations, and there is an urgent need to find more targeted treatment options. Numerous studies have shown that hypoxia is the most important pathogenic factor causing pathophysiological changes in myocardial ischemia. Acute or chronic hypoxia can result in the generation of large amounts of ROS. The outermost layer of each oxygen atom has 2 unpaired electrons, which are highly reactive. Under conditions of hypoxia, excess electrons are provided to oxygen to generate ROS. Oxygen molecules each receive a single unpaired electron to form a superoxide anion radical (O2•–). Acquisition of a second electron generates peroxide, which is then protonated to generate hydrogen peroxide (H2O2); the donation of a third electron via the Fenton reaction results in the generation of a highly reactive hydroxyl group (•OH), and electron leakage further promotes ROS formation [2]. Many studies have suggested that protecting against hypoxia-induced cardiomyocyte apoptosis and necrosis is a potential therapeutic strategy for CHD. Therefore, it is very important to find new therapeutic strategies that can improve the ability of cardiomyocytes to resist ROS and apoptosis under hypoxia [3]. Epidemiological studies have shown that eating more vegetables, fruits, nuts and other healthy plant-sourced foods can significantly reduce the incidence of CHD [4]. The beneficial effects of plant foods against various diseases are partly attributable to the antioxidant and free radical-scavenging properties of polyphenols in foods [5]. Compared with chemical drugs, the phytochemicals in plant foods have relatively weak effects, but herbal medicines are natural antioxidants with great potential for development given their reduced toxicity and side effects. Procyanidins are natural flavonoid polyphenol compounds that are widely distributed in natural products such as fruits, vegetables, nuts, and beans, which are integral parts of the human diet. Their components include monomers (catechin, epicatechin, etc.), oligomers, polymers, and other compounds [6]. The most unique among the various procyanidin forms is the dimer form; the structure of this form gives it a biological activity that is more powerful than that of other water-soluble polyphenols. Thus far, it has been found that the dimer has 8 isomers (B1～8), among which the most active is procyanidin B2 (PB2) [7]. PB2 is a dimer composed of flavan-3-ol and epicatechin. Previous studies have shown that it has antioxidative, anti-inflammatory, and antitumor effects and that it reduces the "three highs". However, whether PB2 is beneficial to cardiomyocyte injury under hypoxic conditions is still unclear. This study lays a foundation for application of PB2 in the cardiovascular system and provides new strategies and ideas for myocardial ischemia and hypoxia treatment.

2. Materials and methods

2.1. Cell culture and PB2 treatment

Human AC16 cardiomyocytes were used from passages 3–8. Normoxic control-group cells were cultured in DMEM at 37 °C under normoxic conditions (21 % O2, 5 % CO2 and 74 % N2), while hypoxia-group cells were cultured in hypoxic Esumi buffer (4 mM HEPES, 117 mM NaCl, 12 mM KCl, 0.9 mM CaCl2, 0.49 mM MgCl2, 20 mM sodium lactate, 5.6 mM 2-deoxyglucose, pH 6.2) at 37 °C, 1 % O2, 5 % CO2 and 94 % N2) for 8 h. Once the cardiomyocytes reached approximately 70 % confluence, they were washed twice with PBS to remove the medium, and 20, 40, or 60 μM PB2 in hypoxic Esumi buffer was added.

2.2. CCK-8 assay

Cell viability was determined by the CCK-8 method. Cells were seeded in 96-well plates, and 6 complex wells were set up in each group, with a cell volume of 4 × 103 per well. Ten microliters of CCK-8 reagent was added to each well, and the cells were incubated for 1 h. The absorbance of the wells was then measured at 450 nm with a microplate reader, and the data were quantified and statistically analyzed to determine relative cell viability.

2.3. Dichlorofluorescein diacetate (DCFH-DA)

The cell culture medium was discarded, and a DCFH-DA probe (diluted to a final concentration of 10 μM in culture medium) was added to each group cells. The cells were incubated in a dark room for 30 min. After thorough staining, the probes that had not entered the cells were washed off with PBS 2 times. After the cells were digested and centrifuged, 500 μL of PBS was added and pipetted to mix. The samples were loaded into a flow cytometer, which was used to measure the fluorescence intensity in the FITC channel.

2.4. Dihydroethidium (DHE) staining

The original cell culture medium was removed, the DHE probe was added to a final concentration of 10 μM, and Hoechst was added at a dilution of 1:100 to each group of cells in culture medium. The cells were then incubated in the dark for 1 h. The probe that did not enter the cells was thoroughly washed off twice with PBS, and the cells were then observed and imaged under fluorescence microscopy.

2.5. BODIPY fluorescence staining

The original culture medium was removed, and the BODIPYTM581/591 C11 fluorescent probe was added to each group of cells in culture medium to a final concentration of 10 μM. After the cells were stained in a dark room for 30 min, the probe that did not enter the cells was washed off with PBS. Then, flow cytometry was used to measure the fluorescence intensity in the FITC channel and PE channel after digestion and resuspension of the cells.

2.6. Annexin V/PI staining

The cell culture medium was discarded, and the cells were washed with PBS. The cells were then digested with EDTA-free pancreatin; DMEM containing 10 % FBS was added to terminate the reaction. After centrifugation, the cells were rinsed with pre-chilled PBS twice, and 500 μL of 1 × Binding Buffer was added to resuspend the cells. Next, 5 μL of Annexin V and 10 μL of PI reagent were added, and fluorescence staining was performed under dark conditions for 15–30 min. The FITC and PE channels were measured by flow cytometry, and scatter plots were drawn.

2.7. TUNEL staining

After the original medium was discarded and the cells were washed twice with precooled PBS at 4 °C, 4 % paraformaldehyde was used to fix the cells. The slides were incubated dropwise with 20 μg/mL Proteinase K solution at room temperature for 5 min, and each sample was incubated with 1 × Equilibration Buffer at room temperature for 10 min. The 1 × Equilibration Buffer was aspirated, and Mix incubation buffer was added dropwise (50 μL Mix: ddH2O 34 μL, 5 × Equilibration Buffer 10 μL, Alexa Fluor 640-12-dUTP Labeling Mix 5 μL, Recombinant TdT Enzyme 1 μL) with protection from light. The cells were then incubated at 37 °C for 60 min. After washing the cells twice with PBS, DAPI-containing mounting agent was added, and the cells were incubated for approximately 5 min. The cells were observed with a fluorescence microscope. Alexa Fluor 640 red fluorescence was measured in the 620 nm channel, and DAPI blue fluorescence was measured in the 460 nm channel.

2.8. JC-1 staining

Working solution preparation: Frozen JC-1 dye was slowly thawed at room temperature, and then 10 μM 1 × working solution was formulated with PBS. The solution was vortexed to mix well. The original culture medium was discarded, and the cells were rinsed with PBS twice. EDTA-free trypsin was added to digest the cells, after which the cells were again washed twice with PBS. Then, 500 μL of JC-1 working solution was added and mixed well, and the cells were incubated for 20 min at room temperature. A flow cytometer was used to measure the fluorescence in the FITC and PE channels, and scatter plots were drawn.

2.9. Western blot analysis

The detailed methodology can be found in our previous publication [8]. Primary antibodies against the following proteins were used in the present study: β-actin (sc-8432, Santa Cruz) and cleaved caspase 3 (#19677-1-AP, Proteintech).

2.10. Transcriptomic study

Transcriptome sequencing: Total RNA was extracted from the two groups of cells after hypoxia treatment, and the RNA concentration and purity were analyzed. The polyA tails of mRNA were used to purify the mRNA from the total RNA. The mRNA was fragmented into 200–300 bp fragments, and cDNA was then synthesized. The fragment size of the cDNA library was set as 300–400 bp, and fluorescence quantification was used to accurately detect the total cDNA concentrations in the library. Automated sequencing was performed on an Illumina sequencing platform. The raw reads were filtered, and the gene sequences obtained after random screening were mapped to different reference genomes for comparison and analysis. According to the results of the comparison, the transcript level of each gene was calculated, and the sequence of each transcript was reproduced after splicing of the corresponding reads.

Differentially expressed gene screening: In this study, DESeq was mainly used to analyze differentially expressed genes. The screening conditions were as follows: $|\log2foldchange|>1$, $p < 0.05$ (considered to indicate significance). The ggplots2 package in the R language was used to draw a volcano map reflecting the obvious differences in gene expression. The R package pheatmap was used to perform cluster analysis on the intersecting differentially expressed genes among all different groups and among samples from each group. The differentially expressed genes in the samples were subjected to multilevel two-way clustering, in which the longest calculation distance method (complete linkage) was used for hierarchical clustering.

Bioinformatic analysis of differentially expressed genes: The Gene Ontology (GO) database includes three important biological

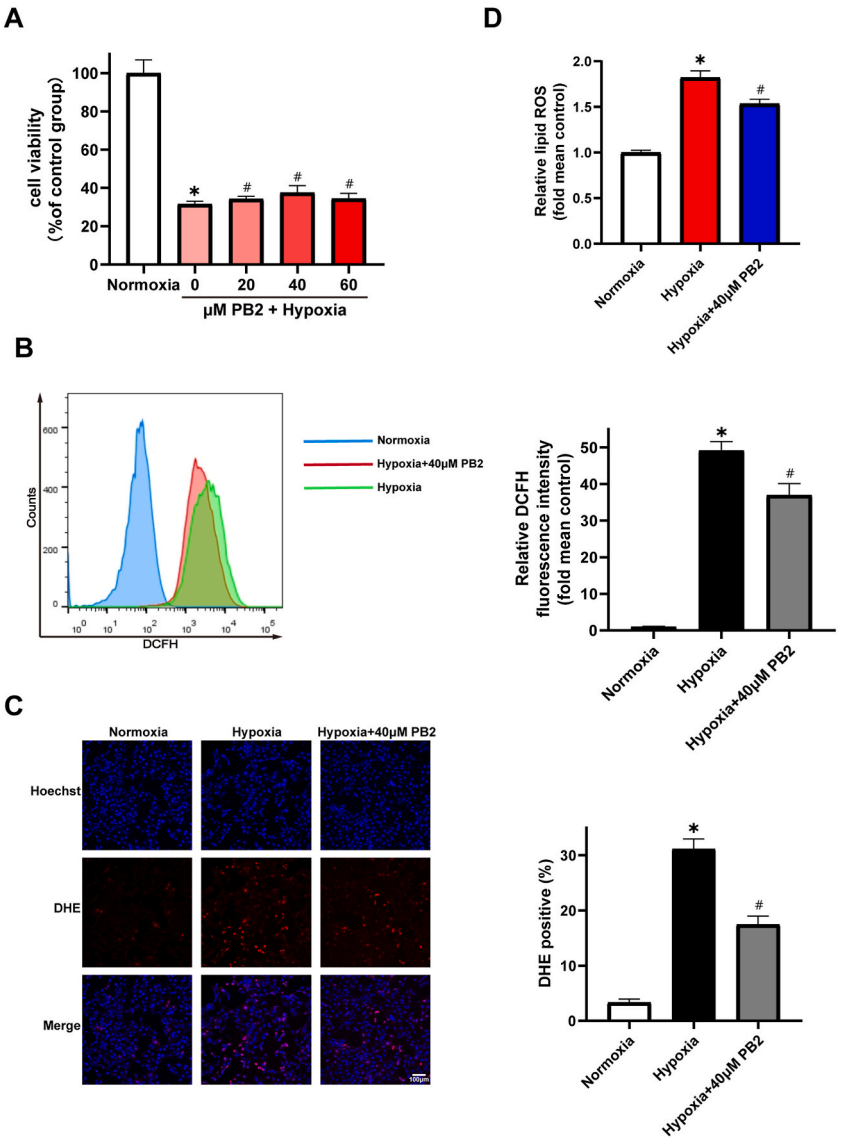

Fig. 1. PB2 increases cardiomyocyte viability and reduces oxidative stress levels under hypoxic conditions. (A) Normoxic control group; hypoxic control group; and 20, 40, and 60 μM PB2 treatment groups under hypoxic conditions. CCK-8 assays were used to measure cell viability. (B) Representative images of DCFH fluorescence staining from flow cytometry and quantification of the flow cytometry results. (C) A fluorescence microscope was used to obtain representative images of DHE fluorescence staining and to perform quantitative analysis of fluorescence results. (D) Quantitative analysis of cellular lipid peroxidation using BODIPYTM581/591 C11. *P < 0.05 compared with normoxic control; #P < 0.05 compared with hypoxic control.

categories: the molecular function (MF), cellular component (CC), and biological process (BP) categories. Genes or proteins can be input as their corresponding symbol annotations to find the corresponding GO numbers [9]. The corresponding GO terms can then be identified. The topGO method was used for enrichment analysis. Briefly, the sequences and numbers of differentially expressed genes that were annotated for each GO term were determined, and then the hypergeometric distribution method was used to calculate the significantly enriched terms. The significant GO terms were used to determine the main biological functions of the differentially expressed genes. The Kyoto Encyclopedia of Genes and Genomes (KEGG) database links information in the genome with higher-level system functions at the cell, species, and ecosystem levels [10]. The various differentially expressed genes obtained according to the screening results were compared to the KEGG database to annotate the altered pathways, and the Fisher test method was used to determine the significantly enriched pathways for the differentially expressed genes.

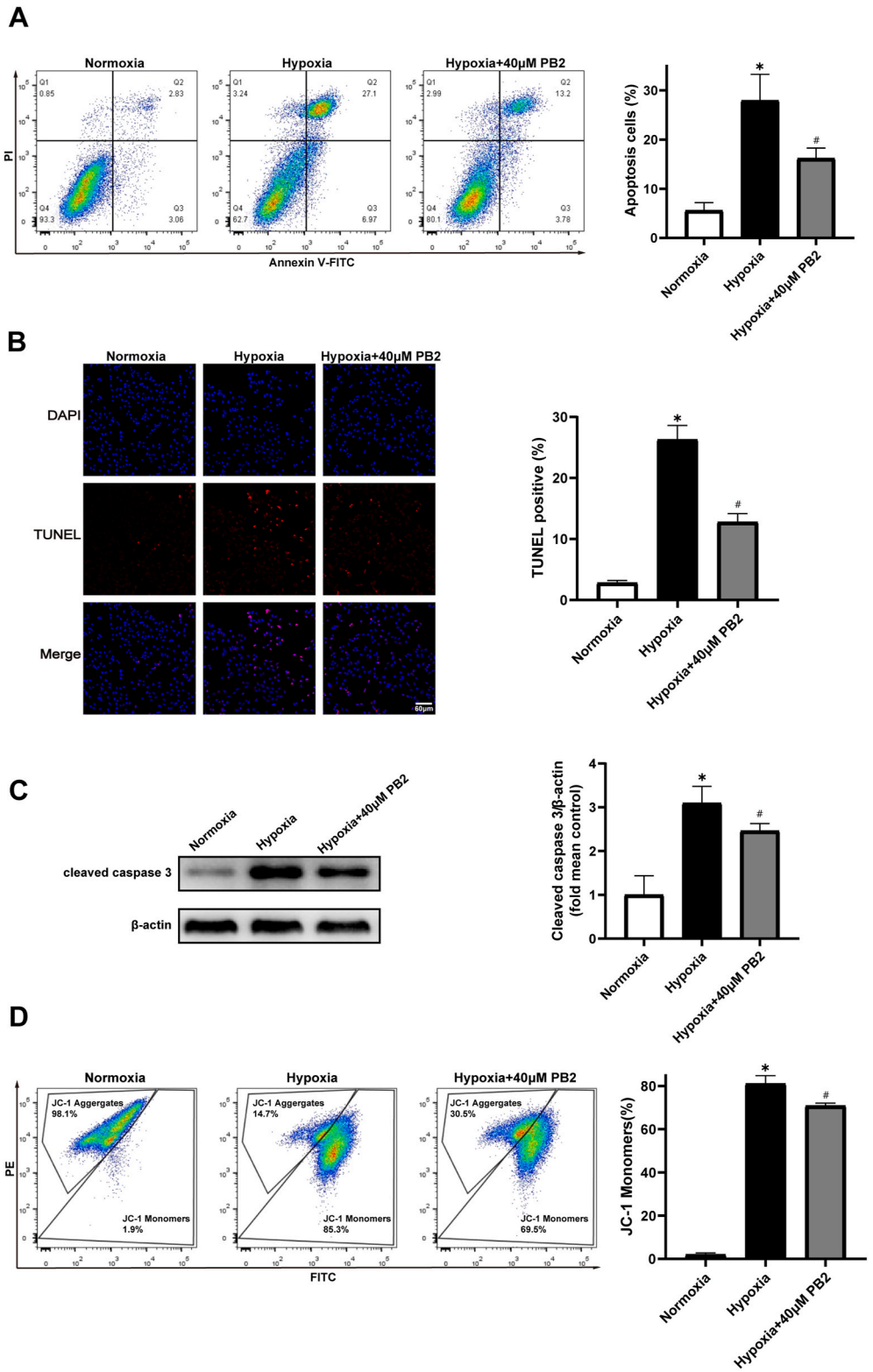

(caption on next page)

Fig. 2. PB2 reduces cardiomyocyte apoptosis and MMP under hypoxic conditions. (A) Annexin V/PI flow cytometry results for apoptosis and representative images. (B) A fluorescence microscope was used to obtain representative images of TUNEL fluorescence staining and to perform quantitative analysis of the fluorescence results. Scale bar, 60 μm. (C) Representative images and relative expression levels of apoptosis marker proteins from Western blotting. (D) Representative graph of MMP measured by JC-1 flow cytometry and statistical analysis of the flow cytometry results. *P < 0.05 compared with normoxic control; #P < 0.05 compared with hypoxic control.

2.11. Metabolomic study

Extensive targeted metabolomics: Liquid chromatography–tandem mass spectrometry (LC−MS/MS), an important method of liquid chromatography−mass spectrometry, can accurately identify and quantify metabolites [11]. The goal of metabolomic analysis is to screen metabolites with biological significance and statistically significant differences from various biological samples and use the results as theoretical bases to explain the altered metabolic processes in organisms [12–14]. The chromatographic column was a 1 mm*100 mm Waters purification column. The mobile phases were as follows: phase A was 0.1 % formic acid in ultrapure water, and phase B was 0.1 % formic acid in acetonitrile. The elution gradient was 0 min, 95:5 water:acetonitrile (v/v); 10.0 min, 10:90; 11.0 min, 10:90; 11.1 min, 95:5; and 14.0 min, 95:5. The flow rate was 0.4 ml/min, the column temperature was 40 °C, and the injection volume was 2 μl. The mass spectrometry conditions mainly included an electrospray ion source temperature of 500 °C, mass spectrometer voltages of 5500 V (+) and 4500 V (−), a GS I pressure of 55 psi, a GS II pressure of 60 psi, a curtain gas pressure of 25 psi, and collision-induced dissociation. The ionization parameter setting was high. Analyst 1.6.3 software was used to analyze the data obtained by mass spectrometry, and the data were then combined with a metabolomics database to quantitatively analyze the metabolites in the mass spectrometry samples. The characteristic ions of each substance were screened by the triple quadrupole method, and the signal intensities of the various characteristic ions were obtained by the detector. The mass spectrum files of the samples were directly opened in Multiquant software for integration and correction of the chromatographic peaks. The top area of each chromatographic peak represented the relative content of the corresponding substance.

Screening of differential metabolites: To accurately discover differential metabolites, multiple statistical analysis methods were used. Orthogonal partial least squares discriminant analysis (OPLS-DA) was the final method used. In multiple variable analysis, the variable importance in the projection (VIP) value obtained from OPLS-DA was used to preliminarily identify metabolites whose levels differed between cell samples. Metabolites with a VIP≥1 were selected, and metabolites with a fold change≥1.5 or a fold change≤0.67 were further screened as differential metabolites.

Bioinformatic analysis of differential metabolites: The KEGG database, a complete scientific information network system, can help researchers comprehensively study information such as gene expression and metabolite levels and is the main public database for the currently known relevant pathways. KEGG analysis enables highly integrated analyses of metabolic pathways including various metabolites (e.g., carbohydrates, nucleosides, amino acids, etc.). The database labels the enzymes that catalyze each step of metabolic reactions and contains links to PDB libraries, etc. This database has become a powerful tool for carrying out metabolomic analysis and metabolic network research.

2.12. Statistical analysis

GraphPad Prism 8 software was used for statistical data analysis and graphing. The data are presented as the mean ± SD. Student's *t*-test was used to analyze the significance of differences between the groups, and P < 0.05 was considered to indicate statistical significance.

3. Results

3.1. PB2 increases cardiomyocyte viability and reduces oxidative stress levels under hypoxic conditions

We used the CCK-8 method to determine the effects of different concentrations of PB2 on cardiomyocyte viability. The cell viability of the hypoxic control group was significantly lower than that of the normoxic control group. However, the cell viability of the groups treated with 20, 40 and 60 μM PB2 under hypoxic conditions was significantly increased. As shown in Fig. 1A, in hypoxic cardiomyocytes, 20 and 40 μM PB2 dose-dependently increased cell viability; however, the viability under 60 μM PB2 was not as high as that under 40 μM. Therefore, we concluded that the concentration of PB2 that exerts a protective effect under hypoxic conditions is approximately 40 μM and used this concentration in subsequent experiments.

ROS are important elicitors of oxidative stress and important causes of pathophysiological changes in myocardial cell ischemia and hypoxia. Therefore, we quantified ROS levels by measuring the relative fluorescence intensity after DCFH-DA staining by flow cytometry. ROS levels in cardiomyocytes were significantly elevated under hypoxic conditions, but the addition of 40 μM PB2 inhibited the ROS elevations (Fig. 1B). DHE is a fluorescent probe that can be used to detect ROS levels from superoxide anion reactions. Quantitative analysis of the percentage of DHE-positive cells confirmed that there were significantly greater numbers of DHE-positive cardiomyocytes under hypoxic conditions than under normoxic conditions but that the hypoxia-induced increase could be inhibited by the addition of 40 μM PB2 (Fig. 1C). BODIPYTM581/591 C11 can be used to detect lipid peroxidation levels in cells and cell membranes, as oxidation of the polyunsaturated interdienyl (C11) of the dye after staining causes the fluorescence emission peak to shift from 590 nm to 510 nm. Therefore, we used flow cytometry to detect the fluorescence intensities of unoxidized C11 (PE

Table 1
Differential genes.

Name	log_2FoldChange	P-value	Stype
EGR1	1.751	2.255E-116	up
C4orf48	1.095	7.338E-09	up
SERPINI1	1.013	8.593E-05	up
TMEM150C	1.003	8.163E-04	up
RHBDL1	1.223	1.189E-03	up
CRLS1	1.536	1.616E-03	up
ADGRB3	1.433	2.980E-03	up
RORB	1.068	3.214E-03	up
NGFR	1.030	4.792E-03	up
CMTM8	1.005	5.191E-03	up
RCAN2	1.763	5.426E-03	up
PCDH10	1.280	5.691E-03	up
DRAXIN	1.131	9.737E-03	up
NPW	1.360	1.083E-02	up
CILP2	1.767	1.090E-02	up
NLGN1	1.166	1.133E-02	up
ADAMTS2	2.227	1.239E-02	up
CRLF1	1.052	1.327E-02	up
PPP1R32	3.308	1.417E-02	up
IFITM10	2.951	1.663E-02	up
UNC13D	2.127	1.828E-02	up
ACP4	1.167	1.855E-02	up
PCDH7	1.072	1.869E-02	up
PDXP	1.864	2.127E-02	up
TIGD3	1.571	2.457E-02	up
FKBP1B	1.590	2.530E-02	up
PTPN5	2.984	2.557E-02	up
ARR3	1.205	2.611E-02	up
TIGD7	1.079	2.620E-02	up
RHD	1.342	2.657E-02	up
SHISA8	1.195	2.727E-02	up
PRR36	1.186	2.846E-02	up
DCDC2B	3.096	2.856E-02	up
RGMA	1.311	3.082E-02	up
MYLK4	1.595	3.088E-02	up
SRXN1	1.342	3.108E-02	up
CACNA1C	1.009	3.292E-02	up
C17orf49	3.020	3.695E-02	up
PLIN1	3.762	3.818E-02	up
IRX6	3.904	3.866E-02	up
C1S	1.749	3.948E-02	up
MTUS2	2.038	3.980E-02	up
RDH5	1.164	4.045E-02	up
DACH1	1.521	4.165E-02	up
DQX1	1.546	4.234E-02	up
MYO1F	1.381	4.282E-02	up
SLC9A3	1.114	4.419E-02	up
TRIM74	1.634	4.535E-02	up
MAP6D1	1.008	4.701E-02	up
USH2A	3.016	4.780E-02	up
RFPL3	2.166	4.797E-02	up
TPBGL	1.261	4.956E-02	up
H2AC19	1.277	4.992E-02	up
PTX3	−1.120	3.421E-58	down
FILIP1L	−1.367	6.883E-50	down
ADGRG1	−1.474	1.097E-46	down
CPA4	−1.008	6.523E-31	down
FGF5	−1.126	1.678E-26	down
TM4SF18	−1.700	2.255E-22	down
CXCR4	−1.023	6.614E-19	down
COL1A1	−1.280	2.780E-17	down
TGM2	−1.265	8.345E-16	down
INHBA	−2.249	1.209E-13	down
SFN	−1.617	1.563E-12	down
FGF1	−1.037	2.606E-12	down
IL24	−1.444	6.529E-11	down
RGS4	−1.456	1.359E-08	down
KRT81	−1.281	7.578E-08	down

(*continued on next page*)

Table 1 (*continued*)

Name	log_2FoldChange	P-value	Stype
KRT75	−1.443	9.871E-08	down
KIF17	−1.223	1.319E-07	down
ABCA1	−1.305	1.643E-07	down
COL16A1	−1.354	1.803E-07	down
EDIL3	−1.255	1.432E-06	down
PTPN22	−1.175	1.457E-06	down
HSD17B2	−1.107	4.763E-06	down
MANSC1	−1.487	7.893E-06	down
KISS1	−1.015	8.030E-06	down
SPON1	−1.105	9.463E-06	down
GLIPR1	−1.068	1.302E-05	down
XDH	−1.041	2.034E-05	down
IGFBP5	−1.716	2.428E-05	down
TSPAN2	−1.281	6.195E-05	down
MYPN	−1.957	6.754E-05	down
LCP1	−1.412	7.725E-05	down
ALPK2	−1.298	1.167E-04	down
IL1B	−1.145	1.412E-04	down
INHBE	−2.733	2.542E-04	down
HKDC1	−1.285	4.121E-04	down
DEPP1	−1.218	4.977E-04	down
DRGX	−2.094	5.803E-04	down
STX1B	−1.311	9.062E-04	down
HCLS1	−2.245	9.551E-04	down
FAT3	−1.375	9.623E-04	down
ABI3	−1.898	9.869E-04	down
TENM2	−2.162	1.328E-03	down
CSF3	−1.201	1.593E-03	down
CCDC198	−2.161	1.794E-03	down
NCF2	−1.080	1.989E-03	down
ZNF860	−1.206	2.423E-03	down
ADGRG4	−1.583	2.649E-03	down
NEURL1	−1.193	2.814E-03	down
LRRTM2	−1.308	3.240E-03	down
SYTL3	−1.321	3.306E-03	down
ISG20	−1.128	3.559E-03	down
HMCN2	−2.079	4.296E-03	down
RUFY4	−4.434	4.987E-03	down
GPR4	−1.124	5.252E-03	down
CCL26	−2.525	5.446E-03	down
DNAH12	−1.439	5.704E-03	down
GRID1	−1.265	6.164E-03	down
NOX4	−1.356	6.594E-03	down
CDK15	−1.099	8.176E-03	down
TAC4	−1.660	8.289E-03	down
MMP10	−2.450	8.650E-03	down
BMPER	−1.499	9.618E-03	down
BLACAT1	−1.279	9.699E-03	down
ADCYAP1R1	−3.129	1.150E-02	down
SH3RF2	−1.151	1.161E-02	down
PLB1	−2.898	1.182E-02	down
IL17B	−1.988	1.254E-02	down
NTNG2	−1.115	1.281E-02	down
NEURL3	−1.406	1.305E-02	down
GJB3	−1.125	1.321E-02	down
MMP19	−2.892	1.405E-02	down
ACP5	−1.840	1.429E-02	down
ATP5ME	−1.412	1.443E-02	down
TBXA2R	−1.139	1.493E-02	down
RSPO2	−1.896	1.493E-02	down
ARL6IP4	−1.936	1.547E-02	down
TNFRSF9	−2.017	1.602E-02	down
IL2RB	−3.368	1.698E-02	down
PADI1	−2.050	2.075E-02	down
TMEM86A	−1.341	2.168E-02	down
CHST4	−1.168	2.253E-02	down
MYO7B	−1.497	2.283E-02	down
TMEM40	−1.082	2.373E-02	down
SCG2	−1.409	2.520E-02	down

(*continued on next page*)

Table 1 (*continued*)

Name	log_2FoldChange	P-value	Stype
ABCB6	−1.243	2.656E-02	down
GBP1	−1.530	2.942E-02	down
PRG4	−1.896	2.962E-02	down
KCNK10	−1.393	3.015E-02	down
TMEM102	−1.227	3.059E-02	down
SPATA25	−1.152	3.173E-02	down
ADRA1D	−1.215	3.366E-02	down
CLDN18	−2.300	3.369E-02	down
MYH1	−1.597	3.409E-02	down
KSR2	−1.018	3.512E-02	down
C16orf95	−1.338	3.766E-02	down
CYP26A1	−1.154	3.796E-02	down
TACR1	−3.133	3.857E-02	down
CNTD1	−1.065	3.916E-02	down
MLXIPL	−3.097	4.029E-02	down
AC013394.1	−1.340	4.103E-02	down
PATE2	−2.688	4.225E-02	down
RGL3	−2.695	4.231E-02	down
OLR1	−3.780	4.516E-02	down
GFAP	−3.782	4.596E-02	down
COL5A3	−1.034	4.932E-02	down

channel) and oxidized C11 (FITC channel), calculated the ratio of the mean fluorescence intensity (MFI) of FITC to the MFI of PE for each sample, and finally obtained the relative lipid peroxidation level for each group. Compared with that in the normoxic control group, the level of lipid peroxidation in the hypoxic group was significantly greater, but the hypoxia-induced increase could be inhibited by the addition of 40 μM PB2 (Fig. 1D).

3.2. PB2 reduces cardiomyocyte apoptosis and mitochondrial membrane potential (MMP) under hypoxic conditions

Cardiomyocyte apoptosis is closely related to myocardial hypoxia damage. Therefore, we used Annexin V/PI fluorescence staining to analyze the apoptosis levels of cardiomyocytes by flow cytometry. We found that apoptosis of cardiomyocytes was significantly greater under hypoxic conditions than under normoxic conditions but that the addition of 40 μM PB2 inhibited the increase in apoptosis (Fig. 2A). Quantitative analysis confirmed that the percentage of TUNEL-positive cardiomyocytes was significantly greater under hypoxic conditions than under normoxic conditions but that this increase could be inhibited by the addition of 40 μM PB2 (Fig. 2B). Quantitative analysis of Western blotting revealed that the expression of the apoptosis-associated protein cleaved caspase-3 in cardiomyocytes was significantly greater under hypoxic conditions than under normoxic conditions but that this increase could be inhibited by the addition of 40 μM PB2 (Fig. 2C).

The level of MMP under hypoxia is closely related to mitochondria-dependent apoptosis, and the MMP is also an indicator of mitochondrial status and function; a significant decrease in MMP usually indicates mitochondrial dysfunction. Quantitative analysis of the percentage of JC-1 monomeric cells after flow cytometry revealed that compared with normoxic control cardiomyocytes, hypoxic cardiomyocytes had a significantly reduced MMP. However, the MMP could be increased by the addition of 40 μM PB2 (Fig. 2D).

3.3. Transcriptomic analysis of the protective effect of PB2 on cardiomyocytes under hypoxia

Cell RNA was extracted from the hypoxic control group and the hypoxic 40 μM PB2-treated group. After the RNA samples were purified and used to generate a library, the library was subjected to paired-end next-generation sequencing on an Illumina sequencing platform [15,16]. The filter conditions for differential expression analysis were as follows: a $|\log2FoldChange|>1$ and a P value < 0.05. A total of 158 differentially expressed genes were obtained with these screening conditions (Table 1), of which 53 genes were upregulated and 105 genes were downregulated. Then, a volcano map was made to show the distribution, expression fold differences and statistical significance of the genes (Fig. 3A). Cluster analysis heatmaps were created to determine the expression patterns of the differentially expressed genes after the addition of PB2 (Fig. 3B). GO enrichment classified the differentially expressed genes according to their MF, BP and CC terms, and the top 10 GO term entries with the smallest p values (the most significant enrichment) were selected for each GO category. The results are shown in Fig. 3C. The degree of GO enrichment was evaluated in terms of the “rich factor”, FDR value and number of genes. The enriched terms included cytokine activity, extracellular matrix, etc. The top 20 GO terms in with the most significant enrichment (lowest FDR values) are displayed in a bubble map in Fig. 3D. In KEGG enrichment analysis, the degree of enrichment was also evaluated in terms of the rich factor, FDR value and number of genes. The enriched pathways included the interleukin (IL)-17 signaling pathway and Jak-STAT signaling pathway. The top 20 KEGG pathways with the most significant enrichment (smallest FDR values) are shown in Fig. 3E.

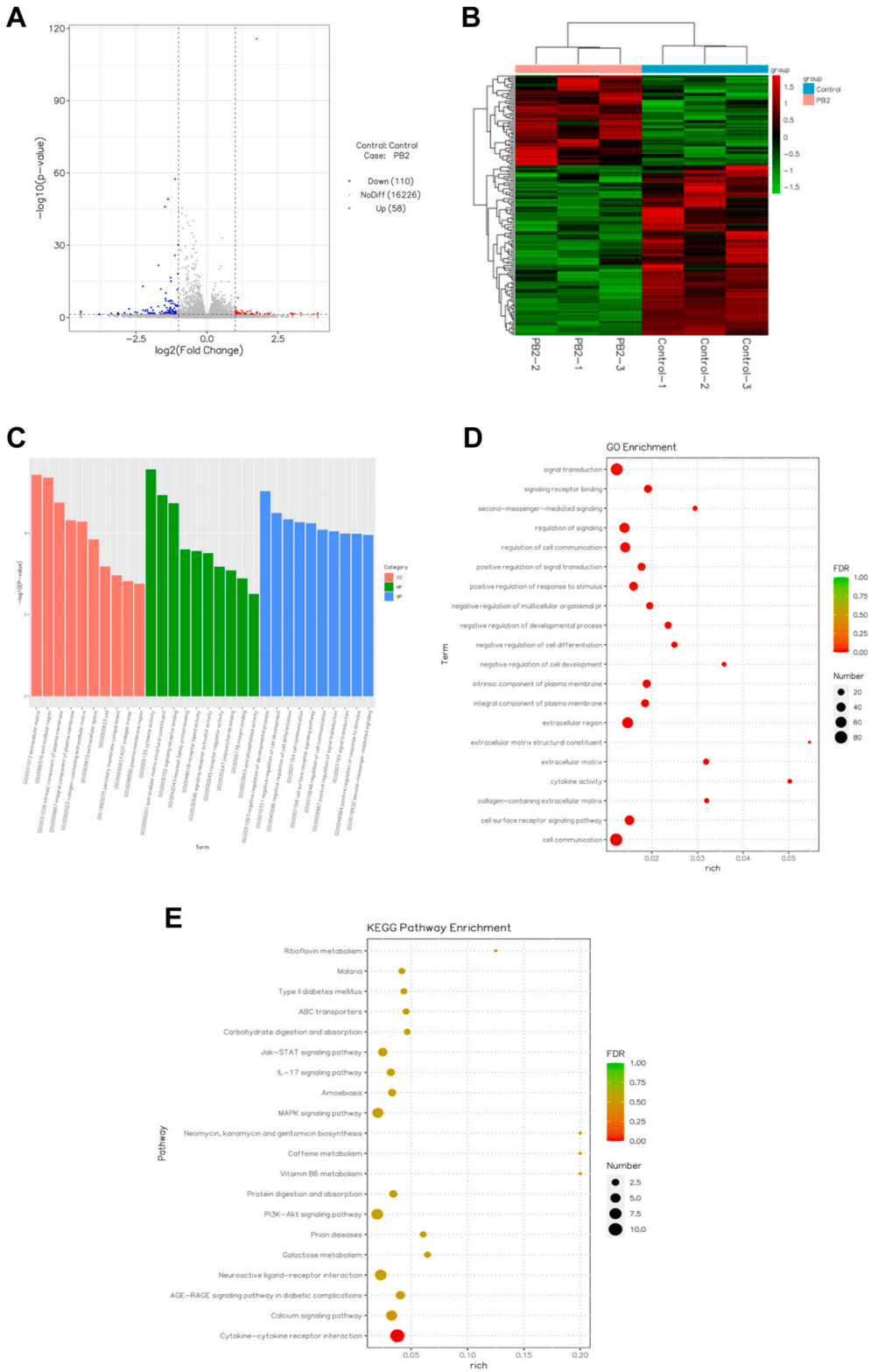

Fig. 3. Transcriptomic analysis of the protective effect of PB2 on cardiomyocytes under hypoxia. (A) Volcano plot of differentially expressed genes. (B) Differentially expressed gene clustering heatmap. (C) GO enrichment analysis histogram. Note: The abscissa is the term in GO level 2, and the ordinate is the -log 10 (P) enrichment value for each term. (D) GO enrichment analysis bubble chart. (E) KEGG enrichment analysis bubble chart.

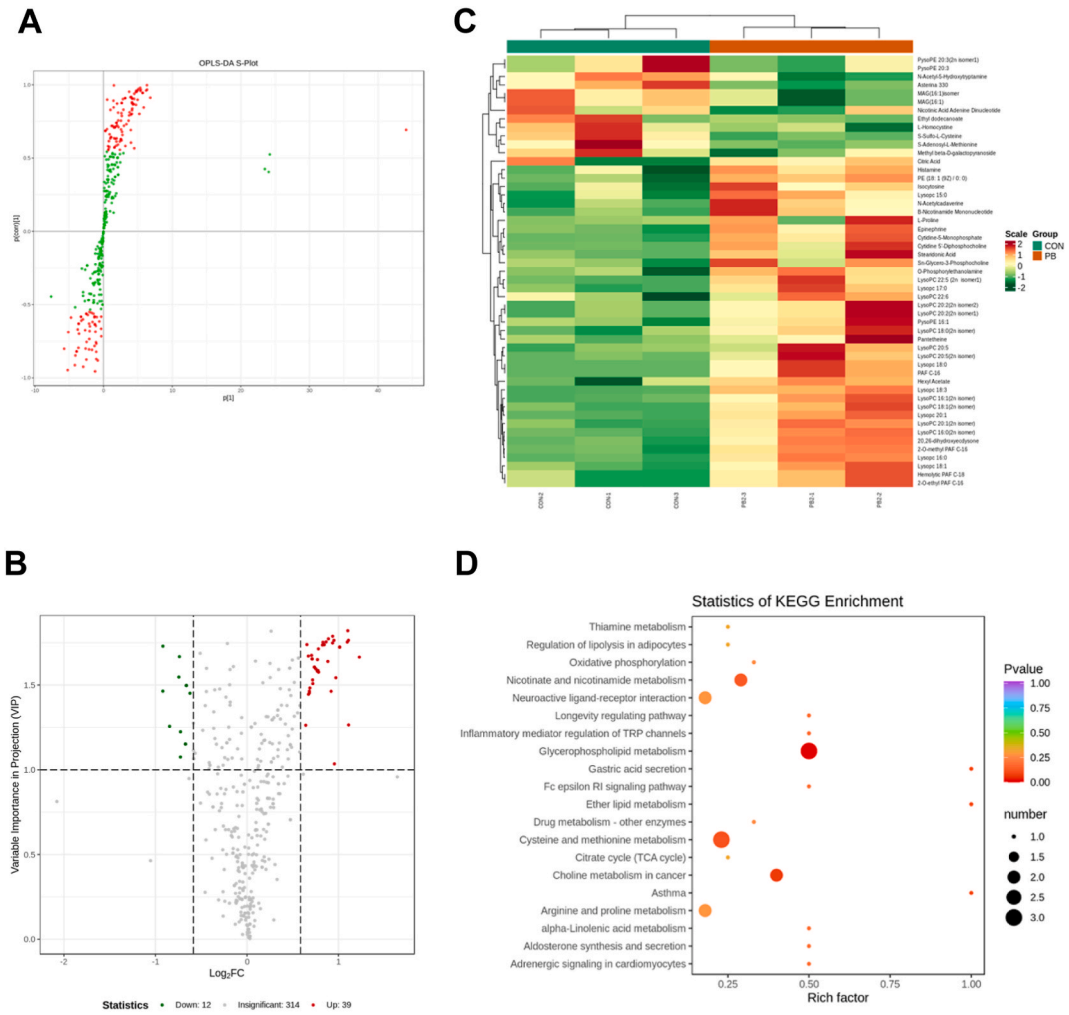

Fig. 4. Metabolomic analysis of the protective effect of PB2 on cardiomyocytes under hypoxia. (A) OPLS-DA S-plot. (B) Volcano plot of differential metabolites. (C) Differential metabolite clustering heatmap. (D) Differential metabolite KEGG enrichment bubble plot.

3.4. Metabolomic analysis of the protective effect of PB2 on cardiomyocytes under hypoxia

According to the OPLS-DA results, an S-plot was drawn (Fig. 4A). The X axis represents the co-correlation coefficient between the principal component and the metabolite, and the Y axis represents the correlation coefficient between the principal component and the metabolite. Metabolites that are closer to the upper right and lower left corners have more significant differences. Each metabolite with a VIP value greater than or equal to 1 is marked with a red dot, while each metabolite with a VIP value less than 1 is marked with a green dot. Differential metabolite screening: The screening criteria were a metabolite fold change≥1.5 or fold change≤0.67. On this basis, metabolites with VIP values ≥ 1 were screened, and a total of 51 differential metabolites were obtained (Table 2). Of these, 39 metabolites had elevated levels, while 12 metabolites had decreased levels. The differences in metabolite levels between the two groups and the statistical significance of the differences were quickly visualized with a volcano plot (Fig. 4B). The significantly different metabolites were normalized with clustering heatmaps (Fig. 4C). KEGG pathway enrichment was carried out according to the results of the differential metabolites, and the enriched metabolic pathways included cysteine and methionine metabolism and arginine and proline metabolism. The top 20 KEGG pathways with the most significant enrichment (smallest p values) are shown in Fig. 4D in a bubble chart.

4. Discussion

Oxidative damage and increased apoptosis of cardiomyocytes caused by hypoxia are important reasons for the poor prognosis of CHD [17]. This study established a hypoxia model of cardiomyocytes and proved that PB2 exerts a protective effect on cardiomyocytes in a hypoxic environment by using CCK-8 experiments. Experiments such as DCFH fluorescence staining, DHE staining, and BODIPY lipid peroxidation detection revealed that PB2 can reduce the oxidative stress levels of cardiomyocytes during hypoxia. TUNEL

Table 2
Differential metabolites.

Compounds	VIP	FoldChange	Type
Citric Acid	1.264	2.159	up
O-Phosphorylethanolamine	1.543	1.961	up
PysoPE 20:3 (2n isomer1)	1.152	0.628	down
PysoPE 20:3	1.152	0.628	down
PysoPE 16:1	1.508	1.647	up
L-Proline	1.035	1.939	up
Histamine	1.464	1.604	up
L-Homocystine	1.451	0.650	down
S-Adenosyl-L-Methionine	1.547	0.597	down
S-Sulfo-L-Cysteine	1.730	0.529	down
Cytidine-5-Monophosphate	1.765	2.157	up
Nicotinic Acid Adenine Dinucleotide	1.076	0.604	down
B-Nicotinamide Mononucleotide	1.639	1.845	up
Epinephrine	1.714	1.718	up
N-Acetyl-5-Hydroxytryptamine	1.464	0.529	down
Lysopc 16:0	1.773	1.853	up
Lysopc 18:0	1.724	2.018	up
Lysopc 18:1	1.675	1.631	up
Lysopc 20:1	1.788	1.914	up
Pantetheine	1.445	1.594	up
Lysopc 17:0	1.736	1.772	up
Sn-Glycero-3-Phosphocholine	1.463	1.892	up
Lysopc 15:0	1.530	1.644	up
Lysopc 18:3	1.821	2.146	up
PAF C-16	1.724	2.018	up
Stearidonic Acid	1.582	1.704	up
Ethyl dodecanoate	1.224	0.604	down
Methyl beta-D-galactopyranoside	1.257	0.556	down
Hexyl Acetate	1.576	1.720	up
Cytidine 5′-Diphosphocholine	1.665	2.342	up
Hemolytic PAF C-18	1.654	1.639	up
PE (18: 1 (9Z)/0: 0)	1.671	1.592	up
2-*O*-ethyl PAF C-16	1.654	1.639	up
N-Acetylcadaverine	1.586	1.713	up
2-*O*-methyl PAF C-16	1.755	1.821	up
20,26-dihydroxyecdysone	1.738	1.796	up
MAG (16:1)isomer	1.497	0.632	down
MAG (16:1)	1.497	0.632	down
LysoPC 22:5 (2n isomer1)	1.754	2.138	up
LysoPC 22:6	1.263	1.561	up
LysoPC 20:1 (2n isomer)	1.749	1.913	up
LysoPC 20:2 (2n isomer 2)	1.605	1.667	up
LysoPC 20:2 (2n isomer1)	1.605	1.667	up
LysoPC 20:5	1.482	1.611	up
LysoPC 20:5 (2n isomer)	1.595	1.685	up
LysoPC 18:0 (2n isomer)	1.650	1.706	up
LysoPC 18:1 (2n isomer)	1.753	1.778	up
LysoPC 16:0 (2n isomer)	1.764	1.933	up
LysoPC 16:1 (2n isomer)	1.739	1.575	up
Asterina 330	1.668	0.599	down
Isocytosine	1.454	1.605	up

staining, Annexin V/PI flow cytometry fluorescence detection, and Western blot assessment of the apoptotic marker protein cleaved caspase-3 confirmed that PB2 can reduce apoptosis of cardiomyocytes under hypoxia, and JC-1 staining showed that PB2 can reduce the MMP of cardiomyocytes under hypoxia.

We performed transcriptomic analysis and found that the expression of a total of 158 genes was significantly changed after PB2 was added to cardiomyocytes during hypoxia. Of the differentially expressed genes, 53 were upregulated and 105 were downregulated. GO enrichment analysis showed that the significantly altered genes were associated with cytokine activity, the extracellular matrix and other biological processes and components, and KEGG enrichment analysis showed that the IL-17 signaling pathway and the JAK-STAT signaling pathway had significant changes. We also performed metabolomic analysis and found that the levels of 51 metabolites in cardiomyocytes were significantly changed after PB2 was added during hypoxia. The levels of 39 of these metabolites were increased, while the levels of 12 of the metabolites were decreased. KEGG enrichment analysis showed that metabolic pathways for cysteine, methionine, arginine and proline were significantly changed.

The IL-17 signaling pathway is emerging as a clinical target in immune-mediated diseases and is associated with significant cardiovascular risk [18,19]. A multicenter prospective study published in Eur Heart J showed that in patients with acute myocardial infarction, serum levels of IL-17 were elevated, and the elevations were associated with an increased risk of major cardiovascular

events [20]. Experimental studies have shown that IL-17 can aggravate ventricular remodeling, increase myocardial infarct size, worsen cardiac function, and increase myocardial fibrosis and cardiomyocyte apoptosis via the p38 MAPK-p53-Bax signaling pathway in the early and late stages after myocardial infarction [21]. At the cellular level, in vitro studies have shown that IL-17 directly induces apoptosis of mouse cardiomyocytes through iNOS activation, which indicates that IL-17 can directly injure cardiomyocytes [22]. Therefore, the downregulation of the IL-17 signaling pathway caused by PB2 may be one of the important mechanisms for the protective effect of PB2 against hypoxia. The finding that the JAK-STAT signaling pathway was downregulated by PB2 is also of great significance. Previous studies have shown that inhibiting JAK-STAT can reduce myocardial cell apoptosis, reduce myocardial infarction remodeling, and inhibit left atrial fibrosis and remodeling after myocardial infarction in mice [23,24]. PB2 may inhibit JAK-STAT phosphorylation and thus become a new drug to improve ventricular remodeling after myocardial infarction.

Regarding metabolic pathways, PB2 supplementation under hypoxia affected the metabolism of cysteine, methionine, arginine, proline, etc. Specifically, the levels of the metabolites L-homocysteine, S-adenosylmethionine, and S-sulfo-L-cysteine were all significantly reduced. Numerous prospective clinical studies have found that elevated homocysteine is an independent risk factor for CHD, and experimental studies have confirmed that feeding mice a high-methionine diet can accelerate the process of atherosclerosis [25–27]. PB2 may reduce cysteine and formazan thionine metabolism, and reducing the synthesis of homocysteine is beneficial to CHD. Regarding arginine and proline, the addition of PB2 increased the levels of proline, an amino acid that is used in protein supplements for malnutrition, burns and surgery and lacks obvious toxicity or side effects. Studies have shown that proline regulates the intracellular redox environment to resist oxidative stress and that proline can maintain NADP/NADPH balance, which contributes to the tricarboxylic acid cycle and GSH biosynthesis [28–30]. Therefore, the increase in proline content may have been one of the reasons for the reduction in oxidative stress in cardiomyocytes after supplementation with PB2 under hypoxic conditions.

In summary, this study proves that PB2 has a protective effect on cardiomyocytes under hypoxia. The signaling pathways and metabolic pathways related to its protective mechanism were preliminarily obtained through transcriptomic and metabolomic analyses and lay a foundation for further research on the effects of PB2 in cardiomyocytes. Our findings also lay a foundation for further research on the role of PB2 in the treatment of CHD and provide new ideas and perspectives for research on PB2 in the treatment of other diseases.

Data availability statement

Data will be made available on request.

CRediT authorship contribution statement

Zhimin Xue: Conceptualization, Investigation, Methodology, Writing – original draft, Writing – review & editing. **Danyu Wu:** Data curation, Investigation, Validation. **Jiefang Zhang:** Formal analysis. **Yiwen Pan:** Software. **Rongsheng Kan:** Writing – original draft. **Jing Gao:** Resources, Visualization, Writing – review & editing. **Binquan Zhou:** Funding acquisition, Project administration.

Declaration of competing interest

The authors declare that they have no known competing financial interests or personal relationships that could have appeared to influence the work reported in this paper.

Acknowledgements

This work was supported by National Natural Science Foundation of China (No.82170330) and Natural Science Foundation of Zhejiang Province (No.LY20H020005).

Appendix A. Supplementary data

Supplementary data to this article can be found online at https://doi.org/10.1016/j.heliyon.2023.e21309.

References

[1] G. Olivetti, R. Abbi, F. Quaini, J. Kajstura, W. Cheng, J.A. Nitahara, E. Quaini, C. Di Loreto, C.A. Beltrami, S. Krajewski, J.C. Reed, P. Anversa, Apoptosis in the failing human heart, N. Engl. J. Med. 336 (1997) 1131–1141.
[2] F.J. Giordano, Oxygen, oxidative stress, hypoxia, and heart failure, J. Clin. Invest. 115 (2005) 500–508.
[3] A.D. Hafstad, A.A. Nabeebaccus, A.M. Shah, Novel aspects of ROS signalling in heart failure, Basic Res. Cardiol. 108 (2013) 359.
[4] A. Satija, S.N. Bhupathiraju, D. Spiegelman, S.E. Chiuve, J.E. Manson, W. Willett, K.M. Rexrode, E.B. Rimm, F.B. Hu, Healthful and unhealthful plant-based diets and the risk of coronary heart disease in U.S. Adults, J. Am. Coll. Cardiol. 70 (2017) 411–422.
[5] Y.J. Zhang, R.Y. Gan, S. Li, Y. Zhou, A.N. Li, D.P. Xu, H.B. Li, Antioxidant phytochemicals for the prevention and treatment of chronic diseases, Molecules 20 (2015) 21138–21156.
[6] D. Bagchi, M. Bagchi, S. Sj, S.D. Ray, C.K. Sen, H.G. Preuss, Cellular protection with proanthocyanidins derived from grape seeds, Ann. N. Y. Acad. Sci. 957 (2002) 260–270.

[7] I. Spranger, B. Sun, A.M. Mateus, F. Vd, J.M. Ricardo-da-Silva, Chemical characterization and antioxidant activities of oligomeric and polymeric procyanidin fractions from grape seeds, Food Chem. 108 (2008) 519–532.
[8] J. Wang, Z. Xue, C. Hua, J. Lin, Z. Shen, Y. Song, H. Ying, Q. Lv, M. Wang, B. Zhou, Metabolomic analysis of the ameliorative effect of enhanced proline metabolism on hypoxia-induced injury in cardiomyocytes, Oxid. Med. Cell. Longev. 2020 (2020), 8866946.
[9] S.Y. Rhee, V. Wood, K. Dolinski, S. Draghici, Use and misuse of the gene ontology annotations, Nat. Rev. Genet. 9 (2008) 509–515.
[10] K. Hashimoto, S. Goto, S. Kawano, K.F. Aoki-Kinoshita, N. Ueda, M. Hamajima, T. Kawasaki, M. Kanehisa, KEGG as a glycome informatics resource, Glycobiology 16 (2006) 63R–70R.
[11] V. Shulaev, Metabolomics technology and bioinformatics, Brief, Bioinformatics 7 (2006) 128–139.
[12] R.J. Bing, A. Siegel, I. Ungar, M. Gilbert, Metabolism of the human heart. II. Studies on fat, ketone and amino acid metabolism, Am. J. Med. 16 (1954) 504–515.
[13] H. Taegtmeyer, L. Golfman, S. Sharma, P. Razeghi, M. van Arsdall, Linking gene expression to function: metabolic flexibility in the normal and diseased heart, Ann. N. Y. Acad. Sci. 1015 (2004) 202–213.
[14] Y. Lv, X. Liu, S. Yan, X. Liang, Y. Yang, W. Dai, W. Zhang, Metabolomic study of myocardial ischemia and intervention effects of Compound Danshen Tablets in rats using ultra-performance liquid chromatography/quadrupole time-of-flight mass spectrometry, J. Pharm. Biomed. Anal. 52 (2010) 129–135.
[15] U. Nagalakshmi, K. Waern, M. Snyder (Chapter 4), RNA-Seq: a method for comprehensive transcriptome analysis, Current protocols in molecular biology (2010) 1–13. Unit 4.11.
[16] M.I. Love, W. Huber, S. Anders, Moderated estimation of fold change and dispersion for RNA-seq data with DESeq2, Genome Biol. 15 (2014) 550.
[17] E. Teringova, P. Tousek, Apoptosis in ischemic heart disease, J. Transl. Med. 15 (2017) 87.
[18] J.W. Williams, L.H. Huang, G.J. Randolph, Cytokine circuits in cardiovascular disease, Immunity 50 (2019) 941–954.
[19] M.D. Mora-Ruíz, F. Blanco-Favela, A.K. Chávez Rueda, M.V. Legorreta-Haquet, L. Chávez-Sánchez, Role of interleukin-17 in acute myocardial infarction, Mol. Immunol. 107 (2019) 71–78.
[20] G. Liuzzo, F. Trotta, D. Pedicino, Interleukin-17 in atherosclerosis and cardiovascular disease: the good, the bad, and the unknown, Eur. Heart J. 34 (2013) 556–559.
[21] S.F. Zhou, J. Yuan, M.Y. Liao, N. Xia, T.T. Tang, J.J. Li, J. Jiao, W.Y. Dong, S.F. Nie, Z.F. Zhu, W.C. Zhang, B.J. Lv, H. Xiao, Q. Wang, X. Tu, Y.H. Liao, G.P. Shi, X. Cheng, IL-17A promotes ventricular remodeling after myocardial infarction, Journal of molecular medicine (Berlin, Germany) 92 (2014) 1105–1116.
[22] S.A. Su, D. Yang, W. Zhu, Z. Cai, N. Zhang, L. Zhao, J.A. Wang, M. Xiang, Interleukin-17A mediates cardiomyocyte apoptosis through Stat3-iNOS pathway, Biochim. Biophys. Acta 1863 (2016) 2784–2794.
[23] H. El-Adawi, L. Deng, A. Tramontano, S. Smith, E. Mascareno, K. Ganguly, R. Castillo, N. El-Sherif, The functional role of the JAK-STAT pathway in post-infarction remodeling, Cardiovasc. Res. 57 (2003) 129–138.
[24] Y. Chen, S. Surinkaew, P. Naud, X.Y. Qi, M.A. Gillis, Y.F. Shi, J.C. Tardif, D. Dobrev, S. Nattel, JAK-STAT signalling and the atrial fibrillation promoting fibrotic substrate, Cardiovasc. Res. 113 (2017) 310–320.
[25] A. Schaffer, M. Verdoia, E. Cassetti, P. Marino, H. Suryapranata, G. De Luca, Relationship between homocysteine and coronary artery disease. Results from a large prospective cohort study, Thromb. Res. 134 (2014) 288–293.
[26] K. Karolczak, W. Kamysz, A. Karafova, J. Drzewoski, C. Watala, Homocysteine is a novel risk factor for suboptimal response of blood platelets to acetylsalicylic acid in coronary artery disease: a randomized multicenter study, Pharmacol. Res. 74 (2013) 7–22.
[27] H.Y. Guo, F.K. Xu, H.T. Lv, L.B. Liu, Z. Ji, X.Y. Zhai, W.L. Tang, J.F. Chi, Hyperhomocysteinemia independently causes and promotes atherosclerosis in LDL receptor-deficient mice, J Geriatr Cardiol 11 (2014) 74–78.
[28] N. Krishnan, M.B. Dickman, D.F. Becker, Proline modulates the intracellular redox environment and protects mammalian cells against oxidative stress, Free Radic. Biol. Med. 44 (2008) 671–681.
[29] X. Liang, L. Zhang, S.K. Natarajan, D.F. Becker, Proline mechanisms of stress survival, Antioxid. Redox Signal. 19 (2013) 998–1011.
[30] H. Takagi, J. Taguchi, T. Kaino, Proline accumulation protects Saccharomyces cerevisiae cells in stationary phase from ethanol stress by reducing reactive oxygen species levels, Yeast 33 (2016) 355–363.